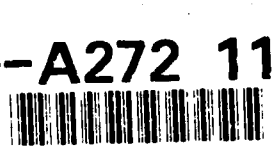

1993 October 15
Quarterly Report
ONR Contract No. N00014-91-C-0128

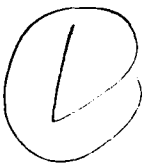

ALCOA TECHNICAL CENTER
100 TECHNICAL DRIVE • ALCOA CENTER, PA 15069-0001

Role of Microstructure on Fatigue Durability of Aluminum Aircraft Alloys

Project Team:
J. R. Brockenbrough
R. J. Bucci
A. J. Hinkle
J. Liu
P. E. Magnusen
S. M. Miyasato

Alcoa Technical Center
100 Technical Drive
Alcoa Center, PA 15069-0001

This document has been approved for public release and sale; its distribution is unlimited.

Creating Value through Technology

CONSTITUENT PARTICLE DISTRIBUTIONS IN 7050 THICK PLATE

S. M. Miyasato
Alloy Technology Division

P. E. Magnusen
A. J. Hinkle
Product Design and Mechanics Division

Alcoa Technical Center
100 Technical Drive
Alcoa Center, PA 15069-0001

ABSTRACT

In some 7050 thick plate, the constituent particle population controls the fatigue crack initiation behavior. Constituent particle distributions were quantified on four microstructural variants of 7050 using automated image analysis. Plate produced with very low microporosity was found to have nearly the same particle distributions as the control plate (standard processing and composition). Plate 1.0 inch thick had the same area fraction of particles measured (~1%), but the large amount of deformation reduced the mean and standard deviation of the particle size. A low mean and standard deviation of the size distribution was achieved in plate with low particle volume fraction. Since the largest values of the particle size distribution affect the fatigue crack initiation behavior, reducing the upper tail of the size distribution is particularly important. Also, although Fe-containing particles were less numerous than Si-containing particles, they were larger and hence are believed to have more influence on fatigue crack initiation behavior.

TABLE OF CONTENTS

INTRODUCTION

Thick plate 7050-T7451 has been the subject of an intense research effort in the area of improved fatigue durability [1-3]. Variants of 7050 were produced through changes in thermomechanical processing history and/or composition to effect changes in microporosity and constituent particle populations. These changes affect the microstructure which in turn may affect the fatigue durability, thus, it is important to characterize the relevant microstructural features. The centerline microporosity in old and new quality 7050 thick plate has been documented [4,5]. This report summarizes the constituent particle distributions in a variety of 7050 products. The characterization of large particles is emphasized, as these control the open hole fatigue lives of some thick plate 7050 product.

These constituent particles, typically Al_7Cu_2Fe and Mg_2Si, form during ingot fabrication. Once these particles form, they are stable, i.e., they cannot be dissolved by thermal practices, and thus persist through to the final product. However, mechanical work does break up the constituent particles: rolling into plate produces long stringers of smaller particles running parallel to the rolling direction. Particles may be up to 100 μm (0.004 inch) in length, and thus are microstructural inhomogeneities from which fatigue cracks may initiate. This report ignores a second class of constituent particles: soluble particles that also form during ingot fabrication, but can be dissolved during thermomechanical processing.

Recent advances in automated image analysis provide a way of obtaining a statistically meaningful characterization of constituent particles. The distribution of particle size is an important material characteristic that conveys more information than the mean value alone. For example, two materials may have the same mean flaw size, but one may have a much narrower size distribution than the other (Figure 1). In 7050 with low levels of microporosity, the microstructural element that controls fatigue damage initiation is constituent particles. Then, the material with the narrower particle size distribution would likely have improved crack initiation resistance, since it is less probable that a large particle would be in a critical area.

In addition to size distribution, spatial distribution can also vary between materials. Two materials may have the same particle size distribution, but the particles may be more clustered in one material. The degree of clustering is also likely to have an effect on the fatigue lifetimes of 7050 thick plate. The distance between particles is easily obtainable using automated image analysis systems.

The development of fatigue durability models of 7050 thick plate require microstructural information, in the form of particle size and spacing distributions. The goal of this work is to provide direct input into micromechanical models enabling prediction of fatigue durability based on microstructure.

EXPERIMENTAL PROCEDURE

Material

Primarily, two samples (both in the -T7451 condition) were used to separate the effects of thermomechanical processing on constituent particle populations. Samples of standard process, new quality material (S. No. 590158) were sectioned to examine the longitudinal plane (normal to the LT direction) for examination at T/10, T/4 and T/2 locations. Similarly, low porosity thick plate (S. No. 590553), produced by proprietary thermomechanical processing, was examined at the various thickness locations. The processing used to reduce the porosity level also affected the grain structure of the plate. The standard processed plate was nominally 5.7 inches thick, and the low porosity plate was 6.0 inches thick.

In addition to these materials, two other variants of 7050 were used to elucidate effects of particle distributions. A low particle plate 6.0 inches thick (S. No. 695474) provided a good comparison with standard plate. (Subsequent work on this variant has been discontinued due to a lack of available material.) A thin plate which is 1.0 inch thick (S. No. 590331) was compared with both the standard 6.0 inch thick plate and the low porosity plate to examine the effect of mechanical work on particle size distribution.

Metallography

Automated quantitative optical metallography was performed on as-polished cross sections of the longitudinal plane to characterize the size and spatial distributions of constituent particles. A low magnification examination (1) maximized the area characterized, and thus improved the chances of encountering the rogue large particles, and (2) degraded the spatial resolution so that closely spaced particles were measured as one particle. Forty fields, each 0.77 mm^2, were analyzed at 100X magnification for a total area of 31 mm^2 (0.048 $inch^2$). An average of 6600 particles was characterized per location in the thickness. Particles smaller than 1.6 μm (0.062×10^{-3} inch) in projected length could not be resolved, and thus were not analyzed.

For irregularly shaped particles, the particle size was defined to be the maximum projected dimension ('DMAX') of the particle since this dimension probably controls the mechanical properties of the material.

Particle spacing ('FERET X') was measured as the surface-to-surface distances parallel to the rolling direction only. While this is not sufficient to uniquely define the spatial distribution of particles in the material, this 'feret distance' does indicate the relative amount of particle clustering in similar samples. Distances larger than a single view field could not be measured, thus providing an upper limit to particle spacing distributions. Speed and cost considerations resulted in the selection of this method over other possible characterization methods. An alternative method that would provide more information would use randomly oriented test lines. The tessellation procedure has also been shown to usefully characterize the degree of particle clustering in low particle volume fraction materials [6].

Quantitative metallography was also done on a similarly designed SEM-based image analysis system. The chemical information collected on the SEM system was used to separate Fe- and Si-containing constituent particles. For these analyses, 20 fields were analyzed at 250X magnification, for a total area of 1.2 mm^2 (0.002 $inch^2$). Particle dimensions as small as 0.4 μm (0.016×10^{-3} inch) were detected.

QUANTITATIVE OPTICAL METALLOGRAPHY

Table 1 contains the results of the quantitative optical metallography at various thickness locations in standard processed (S. No. 590158) and low porosity (S. No. 590553) plate. The particle area fraction, number density, size and spacing on the standard processed plate will be discussed first, then comparisons between the two products will be made in the following section.

Through-Thickness Effects

Through-thickness effects can be seen by comparing particle distributions at the T/10, T/4 and T/2 locations. The particle distribution is expected to vary with location for two reasons. First, Fe and Si solute segregate during casting, with the peak solute content typically occurring at ~T/4. Also, the local amount of hot deformation absorbed during hot rolling varies inversely with plate depth, which affects the particle size, shape and number density.

In the standard plate, the area fraction of constituent particles larger than 1.6 μm varied only slightly between T/10, T/4 and T/2 locations, as shown in the bar graph in Figure 3a. The T/10 location had the largest area fraction of particles (1.31%), while the T/2 location had the smallest (0.99%). Since the area fraction was calculated by computing the area fraction for each of the forty fields, then averaging those values, another important value is the standard deviation (indicated by arrows in Figure 3a), which indicates the field-to-field microstructural variability. The large standard deviations suggest a nonuniform distribution of particles through the material, even when examining only one location in the thickness; this emphasizes the importance of characterizing sufficient area to overcome the inherent variability in constituent particle population.

The number of particles observed decreased monotonically with depth in the plate (Figure 3b). Since the number of particles decreased by almost 50% from the T/10 to T/2 location while the area fraction stayed nearly the same, the mean particle size increased with through-thickness location. This is consistent with the slower cooling rate during solidification, as well as the decreased amount of deformation absorbed during rolling, with increased depth in the thick plate.

Figure 4a displays the distribution of particle sizes for the different plate locations on a logarithmic scale; this same information is also included in Table 2. The T/10 location is seen to have almost twice as many small (<10 μm) particles as the T/4 and T/2 locations. However, all three locations showed about the same number of large particles. The histograms in Figure 4 demonstrate the truncation of the particle size distribution. Since the particle size distribution is cut off at the resolution limit of the image digitizer, the results cannot be fit to a normal distribution in a valid way. Thus, the mean and standard deviation values reported in Table 1 are representative of the particles 1.6 μm or larger, and are not representative of the actual particle population in the material. This calculated mean particle size is therefore an overestimate of the actual value, since the mean value would decrease with the addition of smaller particles to the distribution. These calculated values can be used to compare materials characterized in this study, but comparisons with data reported elsewhere should be made cautiously.

There was a trend towards decreasing mean particle spacing (feret x distance) in the rolling direction with plate depth (Table 1). 'Particle spacing' encompassed two lengths: an inter-particle spacing of relatively short lengths for a stringer of particles, and an inter-stringer spacing of relatively large lengths. Histograms of particle spacing (Figure 5a and Table 3) show that the plate location has a strong effect on the high end, inter-stringer spacings. At the T/10 location, a large number of long spacings were observed compared to the T/2 location, corresponding to the higher amount of hot rolling deformation absorbed near the plate surface. At the smaller particle spacings, there seemed to be less of an effect of location on the inter-particle spacings.

Effect of Processing

Comparison between standard plate and low porosity plate shows the effect of the processing path on constituent particle distributions. Figure 3a graphically indicates the area fraction of particles in the low porosity plate. The area fraction of constituent particles was lowest at the T/2 location, with a value of 0.98%. In comparing the processing methods, there was little difference in the particle area fraction at the various locations. The number of particles was consistently lower in the low porosity plate than in the standard processed plate (Figure 3b), suggesting that there may have been more large particles in the low porosity plate. Figure 4b shows the particle size distribution for low porosity plate. The size distributions produced in standard processed and low porosity plates strongly resemble each other, which suggests that the differences in processing between these two types of 7050 thick plate have little effect on the particles.

The particle spacing in the low porosity plate followed trends similar to those observed in standard processed plate (Figure 5b). The location had a strong effect on the inter-stringer spacings, but a weak effect on the inter-particle spacings.

To summarize, the processing path had only small effects on the constituent particle size and spatial distributions. Both standard and low porosity plate processing produced particle area fractions that were lowest at the T/2 location, number densities that were lowest at the T/2 location, and inter-stringer spacings that were largest at the T/10 location. The similarities between the two products are reasonable, since the processing path used to produce the low porosity plate were not expected to significantly affect the constituent particles.

The effect of low porosity processing was much less than the effect of through-thickness location, which also shows the effect of processing. The higher amount of deformation absorbed by the T/10 location produces particles with a smaller mean size and larger average particle spacing.

Particle Size Distribution

Probabilistic fracture mechanics incorporating microstructural information requires quantification of the particle size distribution. One way to represent the data is to normalize the frequency of particle size by the number of particles measured at that depth. Figure 6 shows the resulting plot of normalized frequency versus particle size in both standard and low porosity materials at the three different locations. The low ends of the particle size distributions were not affected by either the thickness location or the type of material. The distributions do show greater divergence at the larger particle sizes: the T/2 locations have a higher percentage of larger particles than the T/10 locations.

The constituent particles were irregular in shape, and thus it was of interest to check whether the actual area of the particles followed the same behavior as the longest projected dimension. Because the image analyzer captured the real cross-sectional area of the particles, it was not necessary to make assumptions about the particle shape. Figure 7 displays the probability plots for the particle area, which follow the same characteristic curve as the longest projected dimension plots in Figure 6. As was found for particle length, the smaller particles showed no effect of either thickness location or the type of material, and the divergence increased with particle size. The distributions for both standard and low porosity material were slightly narrower at the T/10 plate depth than the T/2. Although particle length and area are equally easy to obtain in automated image analysis, length will continue to be used to characterize particles.

Sample Size

In these materials, the low volume fraction of particles requires that a large sample area be characterized for precise, accurate quantification. Extensive characterization, however, can be time-consuming and expensive even with automated image analysis. Thus, the T/2 locations in both standard and low porosity materials were also analyzed using a smaller sample area (Table 4). This was done on an SEM by increasing the magnification from 100X to 250X and reducing the number of fields from 40 to 20, which reduced the area of material characterized by over 12 times. Since both the magnification and the number of fields were changed, the effect

of analyzed area alone could not be deconvoluted. An experiment comparing different areas at the same magnification, or measuring the same area using different magnifications, should be performed in the future. With this caveat, the following are some comments that can be made.

The particle area fraction when measured at the lower magnification (100X) is significantly higher for both standard and low porosity materials, despite the fact that a large number of particles were below the resolution limit when using the lower magnification (over 50% of the particles measured at 250X were below the detection limit at 100X). For example, the area fraction of constituent particles in low porosity material was 0.98% at 100X and 0.55% at 250X. The resolution limit at the lower magnification may have partially contributed to the higher area fraction, since the matrix area between closely spaced particles may be measured as particle area. Another possible factor is that the limited sampling at 250X was not representative of the total population. Since constituent particles are not uniformly distributed through the material, a large area must be sampled to experimentally characterize the high-end tail of the particle size distribution.

Figure 8 compares the particle size distributions measured at the different magnifications. For both standard processed and low porosity materials, the higher magnification (250X) resulted in a lower median particle size. This also stems at least partially from the fact that particles separated by very small distances may be measured separately at the higher magnification but measured together as one large particle at the lower magnification. One consequence is that the particle number density be greater for the higher magnification analysis, which is indeed the case: standard material had 166 particles/mm^2 at 100X and 259 particles/mm^2 at 250X.

QUANTITATIVE SEM METALLOGRAPHY

The SEM-based automated image analysis system can collect similar data separated by chemical composition. This provides additional information on the particle distributions in standard and low porosity plate. The next section describes the particle distributions characterized from SEM images in standard and low porosity plate. Then, the last two sections include information obtained for two other material conditions, the low particle variant of 7050 (S. No. 695474) and the 1 inch thick plate (S. No. 590331).

Fe and Si Distributions

Since the primary insoluble constituents in 7050 are Al_7Cu_2Fe and Mg_2Si, particles were characterized as either Fe-containing or Si-containing. Table 5 contains the image analysis data from standard and low porosity plate, at the midthickness location, obtained from SEM images at 250X over a sample area of 1.2 mm^2. A relatively small number of particles (around 300) were analyzed in standard and low porosity plate, and more than half of the particles were Si-containing in both plate products.

The histograms in Figure 9 indicate the size distributions for Fe-containing and Si-containing particles. The Si-containing particle distributions are skewed left to the smaller end on the logarithmic plots, while the Fe-containing particles are more normally distributed. The trends for the Si- and Fe-particle sizes are particularly dramatic for the low porosity plate. Because the Si-containing particle distribution is truncated, the mean value reported in Table 5 is an overestimate of the mean of the actual particle distribution. In contrast, the Fe-containing particle distribution does not appear to be significantly truncated.

The normalized plots for standard processed and low porosity plates (Figure 10) also show the difference in size between types of particles. The thick solid line represents the total constituent particle population. For both processing paths, the Fe-containing particles lie to the right, indicating larger sizes, and the Si-containing particles lie to the left, indicating finer sizes. Thus, although Si particles are more numerous, they are smaller and may not play as significant a role as Fe containing particles on fatigue crack initiation.

Effect of Low Particle

Comparisons between standard and low porosity plate provide an understanding of the effect of processing on constituent particles. It is also of interest to explore the large reduction in both particle area fraction and particle number density in S. No. 695474 (Table 5). The area fraction in the standard processed plate was 0.304%, and that for low particle plate was 0.071%. The number density of particles decreased from 259 particles/mm^2 in the standard plate to 164 particles/mm^2 in the low particle plate.

Comparison of the particle size histograms for standard plate and low particle plate (S. No. 695474) reveals a difference in the particle size distributions (Figure 11). The number of particles in low particle plate drops off dramatically with particle size; very few particles are larger than 5.5 μm. This contrasts with the more uniform distribution of particle sizes in standard plate. It is important to note that the low particle plate has not only a smaller area fraction of particles, but also a smaller mean particle size and a narrower particle size distribution. The narrower distribution should produce an improvement in fatigue crack initiation, which depends on the probability of a large flaw being in a certain area.

In addition to having a higher mean particle size, Fe-containing particles also have a higher standard deviation than Si-containing particles. Because of the higher number density of Si-containing particles, the total particle population closely resembles the population of Si-containing particles.

Thin Plate Results

Quantification of the particles at T/2 in thin plate, i.e., 1.0 inch thick, provided an opportunity to study the effect of high amounts of deformation. These results complement the study of different through-thickness locations presented earlier in this report. The T/10 location in 6.0 inch thick plate has absorbed more deformation than the T/2 location; however, the centerline position in 1.0 inch thick plate has absorbed even larger amounts of deformation and has a different particle size distribution. In the thin plate (S. No. 590331), the area fraction of particles was roughly the same as for both the standard processed (S. No. 590158) and low porosity (S. No. 590553) thick plate materials. However, the number of particles was three times as large as for standard and low porosity plate due to the large amount of deformation absorbed during rolling down to 1.0 inch thick plate compared to rolling down to 6.0 in thick plate. Figure 11(b) graphically shows the high number density in the 1 inch thick plate. The increased deformation breaks up the larger particles and refines the particle size distribution. The mean area of individual particles dropped from 11 μm^2 in standard processed plate to 5.3 μm^2 inch in thin plate. The particle number density increased from 259 particles/mm^2 in standard plate to 768 particles/mm^2 in the 1 inch thick plate.

Figure 12 (b) shows the cumulative distribution of Fe- and Si-containing particles, normalized by the number of particles of each type. The Fe-containing particles are still larger than the Si-containing particles even after high amounts of deformation. Thus, even though the Fe-containing particles are initially larger than the Si-containing particles, the Fe particles are not

broken down to the same size distribution as the Si particles. Instead, the Fe particles consistently retain a larger size than the Si-containing particles. The mean particle size was also smaller in high deformation plate compared to standard and low porosity plate. Nonetheless, the variant with the finest particles was the low particle plate.

In the thin plate particles lay in stringers, and it is possible that these clusters of particles act to initiate fatigue cracks, rather than individual particles. Unfortunately, no measure of the spatial distribution was obtained during the SEM-based image analyses. It is postulated that both the inter-particle and inter-stringer distances increased with the increased amount of deformation, which may have also improved fatigue crack initiation resistance. Future work should include measuring the degree of clustering in thin plate.

As expected, the aspect ratio of the particles did not change with amount of deformation. The mean aspect ratio of all particles in standard processed plate was 0.52, and the mean aspect ratio in thin plate was 0.53.

SUMMARY

Based on the results of automated image analysis on the constituent particles in the four microstructural variants of 7050-T7451 product, the following conclusions can be made:

1. The area fraction of constituent particles in all the standard 7050 materials was around 1%. A great deal of scatter was observed in the area fraction data.

2. The processing path used to produce low porosity thick plate did not significantly affect the area fraction of constituent particles. However, very high amounts of deformation, such as used to produce 1.0 inch thick plate, did affect the number density of particles, particle size, mean value, and standard deviation.

3. Low particle plate had both a smaller mean particle size and a narrower the particle size distribution.

4. Si-containing particles were more numerous than Fe-containing particles, sometimes by a factor of two. However, the Fe particles were larger than the Si particles, and may thus have a more significant effect on deformation and fracture.

5. Although a significant number of particles may be below the resolution limit at 100X, large particles are better characterized at this low magnification than at higher magnifications, since more sample area can be covered in the same amount of time.

PROGRAM STATUS

The particle distribution data, which are measured metallographically on random plane sections through the material, serve as the starting point for probabilistic analyses of fatigue performance based on material microstructure. Fatigue crack initiation is controlled by the largest particles, or the extreme value distribution of particle sizes. To obtain predictions of fatigue performance based on the measured distributions, it is necessary to first calculate the extreme value distribution of particle sizes from the measured population in the material. Methods of scaling the measured particle size distribution to obtain the extreme value distribution have been developed. The calculated extreme value distribution closely matches the distribution of fatigue initiating features which is measured from the fracture surfaces of failed fatigue specimens. The extreme value distributions are then input into fatigue models enabling prediction of the fatigue performance of the material.

ACKNOWLEDGMENTS

This work was funded by the Office of Naval Research under Contract Number N00014-91-C-0128. We thank Dr. A. K. Vasudevan, the ONR program manager. Thanks are also due to J. A. Schelin, who provided material and composition and processing information. Thanks are also due to D. H. Ringer for sample preparation, and to B. J. Johnson and R. H. Borland for quantifying the particle distributions. T. N. Rouns helpfully provided numerous suggestions on analysis methods.

REFERENCES

1. C. R. Owen, R. J. Bucci and R. J. Kegarise, "Aluminum Quality Breakthrough for Aircraft Structural Reliability," *J. Aircraft*, Vol. 26, No. 2, February 1989, pp. 178-184.

2. P. E. Magnusen, R. J. Bucci, A. J. Hinkle, R. L. Rolf and M. E. Artley, "The Influence of Material Quality on Airframe Structural Durability," Advances in Research, Vol. 2, Fatigue, Creep and Environmental Fracture, Proc. 7th Int. Conf. on Fracture (ICF), Houston, TX, 1989-03-20 through 03-24, pp. 999-1006.

3. P. E. Magnusen, A. J. Hinkle, R. J. Bucci, R. L. Rolf and D. A. Lukasak, "Methodology for the Assessment of Material Quality Effects on Airframe Fatigue Durability," Fatigue 90, Vol. IV, Proc. 4th Int'l. Conf. on Fatigue and Fatigue Thresholds, Materials and Component Engineering Publications Ltd., Birmingham, UK, pp. 2239-2244, 1990.

4. A. J. Hinkle, P. E. Magnusen, R. L. Rolf and R. J. Bucci, "Effect of Microporosity on Notched Specimen Fatigue Life," Structural Safety & Reliability, Proceedings of ICOSSAR '89, 5th Int'l conf., San Francisco, CA, 1989 08-07 through 08-11, Am. Sco. Civ. Eng., New York, NY, pp. 1467-1474.

5. A. F. Grandt, Jr., A. J. Hinkle, T. D. Sheumann and R. E. Todd, "Fatigue and Fracture of Engineering Materials and Structures," 1991-09-30.

6. T. N. Rouns, J. M. Fridy, K. B. Lippert, O. Richmond, "Quantitative Characterization and Modeling of Second Phase Populations Through the Use of Tessellations," Simulation and Theory of Evolving Microstructures, ed. M. P. Anderson and A. D Rollet, TMS 1990, pp. 269-275.

Table 1. Select parameters for constituent particles in two 7050 materials, showing the effect of plate location and processing. Analysis was performed at 100X magnification.

Feature	Standard (S. No. 695158)			Low Porosity (S. No. 695553)		
	T/10	T/4	T/2	T/10	T/4	T/2
area fraction						
mean, %	1.31	1.17	0.99	1.17	1.21	0.98
std dev, %	0.17	0.16	0.18	0.12	0.21	0.18
no. of particles	9376	6495	5136	7977	6330	4256
particle density, mm^{-2}	303.1	210.0	166.0	257.9	204.6	137.6
longest dimension						
maximum, μm	80.2	95.8	90.4	53.4	86.0	108.3
mean, μm	10.3	12.0	12.0	10.2	11.9	12.7
std dev, μm	± 5.5	± 7.4	± 7.7	± 5.3	± 7.2	±9.3
aspect ratio						
mean	0.587	0.565	0.587	0.616	0.587	0.596
std dev	0.167	0.178	0.171	0.164	0.175	0.170
area						
mean, μm^2	42.0	54.2	57.6	44.2	57.5	67.2
std dev, μm^2	34.4	55.9	60.3	36.6	59.8	82.8
perimeter						
mean, μm	28.8	33.2	33.9	29.1	33.7	36.1
std dev, μm	14.7	20.8	22.2	14.5	20.9	26.7
feret x distance						
mean, μm	198	191	172	195	173	164
std dev, μm	198	204	211	200	208	214

jw/3382

Table 2. Number of particles counted in standard and low porosity materials in the specimen area of 31 mm^2.

Particle Size		Standard (S. No. 695158)			Low Porosity (S. No. 695553)		
μm	log (μm)	T/10	T/4	T/2	T/10	T/4	T/2
4.8978	0.69	1401	775	643	1215	767	645
6.0256	0.78	2047	1135	936	1664	1108	711
7.4131	0.87	1420	867	688	1304	832	518
9.1201	0.96	1607	1066	829	1377	1038	606
11.220	1.05	1125	809	554	865	783	457
13.804	1.14	808	697	562	698	670	405
16.982	1.23	494	467	374	449	470	351
20.893	1.32	259	329	249	242	336	209
25.704	1.41	132	184	156	112	189	170
31.623	1.50	56	92	83	40	79	93
38.905	1.59	19	49	33	8	39	40
47.863	1.68	5	17	19	3	12	34
58.884	1.77	1	5	6	0	4	7
72.444	1.86	2	1	3	0	3	6
89.125	1.95	0	2	1	0	0	4

Table 3. Number of particle spacing counted in standard and low porosity materials in the specimen area of 31 mm^2.

Particle size		Standard (S. No. 695158)			Low Porosity (S. No. 695553)		
μm	log (μm)	T/10	T/4	T/2	T/10	T/4	T/2
1.26	0.100	110	84	78	82	111	67
1.96	0.293	83	57	80	69	90	63
3.07	0.487	68	76	58	60	75	64
4.79	0.680	48	60	46	49	58	36
7.47	0.873	112	110	87	102	111	81
11.66	1.07	73	75	72	83	94	75
18.20	1.26	100	71	71	108	112	86
28.40	1.45	146	90	62	96	99	64
44.33	1.65	138	91	71	100	94	75
69.18	1.84	196	113	71	171	124	59
108.0	2.03	268	194	95	250	140	100
168.5	2.23	323	205	132	286	168	92
263.0	2.42	376	238	143	281	207	126
410.5	2.61	292	223	123	242	179	101
640.8	2.81	85	69	60	84	84	58

jw/3382

Table 4. Comparison of particle distributions obtained at 100X (sample area 30.9 mm^2) on optical images and 250X (sample area 1.24 mm^2) on SEM images.

	Standard (S. No. 590158)		Low Porosity (S. No. 590553)	
	100X	250X	100X	250X
area fraction				
mean, %	0.99	0.30	0.98	0.55
std dev, %	0.18	0.15	0.18	0.45
no. of particles	5136	312	4256	339
particle density, mm^{-2}	166.0	258.7	137.6	281.1
longest dimension				
maximum, µm	90.4	31.1	108.3	44.8
mean (normal), µm	12.0	5.3	12.7	5.8
std dev (normal), µm	± 7.7	± 4.7	± 9.3	± 5.6
aspect ratio				
mean	0.59	0.52	0.60	0.56
std dev	± 0.17	± 0.20	± 0.17	± 0.17
area				
mean, μm^2	57.6	11.0	67.2	18.2
std dev, μm^2	± 60.3	± 16.5	± 82.8	± 38.0
perimeter				
mean, µm	33.9	14.6	36.1	16.4
std dev, µm	± 22.2	± 13.1	± 26.7	± 17.3

jw/3382

Table 5. SEM image analysis data obtained on four 7050 materials, separating Al_7Cu_2Fe and Mg_2Si particle distributions.

	Standard (S. No. 590158)			Low Porosity (S. No. 590553)		
	all	Fe	Si	all	Fe	Si
area fraction						
mean, %	0.304	0.187	0.090	0.551	0.379	0.118
std dev, %	0.153	0.099	0.079	0.449	0.425	0.077
no. of particles	312	138	170	339	137	199
particle density, mm^{-2}	259	111	137	281	111	161
longest dimension						
maximum, µm	31.1	25.0	31.1	44.8	44.8	28.1
mean (normal), µm	5.3	6.9	4.1	5.8	9.0	3.7
std dev (normal), µm	±4.7	±5.0	±4.0	±5.6	±6.4	±3.6
aspect ratio						
mean	0.52	0.51	0.51	0.56	0.52	0.59
std dev	±0.20	±0.20	±0.20	±0.17	±0.17	±0.17
area						
mean, μm^2	11.0	16.8	6.5	18.2	34.3	7.3
std dev, μm^2	±16.5	±19.7	±11.7	±38.0	±52.6	±16.2
perimeter						
mean, µm	14.6	19.3	11.0	16.4	25.5	10.3
std dev, µm	±13.1	±14.8	±10.2	±17.3	±21.5	±9.7

	Low Particle (S. No. 695474)			Thin (S. No. 590331)		
	all	Fe	Si	all	Fe	Si
area fraction						
mean, %	0.071	0.021	0.047	0.427	0.184	0.210
std dev, %	0.057	0.016	0.050	0.111	0.085	0.054
no. of particles	198	48	150	926	206	714
particle density, mm^{-2}	164	38	121	768	166	577
longest dimension						
maximum, µm	11.8	7.4	11.8	24.5	24.5	14.0
mean (normal), µm	3.0	3.7	2.8	3.6	5.8	3.0
std dev (normal), µm	±1.8	±1.8	±1.8	±2.6	±3.5	±1.9
aspect ratio						
mean	0.60	0.55	0.61	0.53	0.45	0.55
std dev	±0.17	±0.15	±0.17	±0.19	±0.17	±0.18
area						
mean, μm^2	4.2	5.4	3.9	5.3	11.1	3.6
std dev, μm^2	±5.3	±3.8	±5.6	±8.4	±14.6	±4.1
perimeter						
mean, µm	8.5	10.1	7.9	9.6	15.2	8.0
std dev, µm	±4.9	±4.7	±4.9	±7.0	±10.1	±4.6

jw/3382

Table 6. Frequency of particles counted in the various 7050 product, as characterized on the SEM at 250X.

Particle Size		Standard (S. No. 590158)			Low Porosity (S. No. 590553)		
µm	log (µm)	total	Fe	Si	total	Fe	Si
1.26	0.10	33	7	26	35	3	31
1.61	0.21	42	10	32	55	6	49
2.06	0.31	34	13	21	34	5	29
2.63	0.42	35	11	24	35	4	31
3.36	0.53	37	10	27	24	10	14
4.30	0.63	27	19	8	28	16	12
5.50	0.74	19	12	7	30	21	9
7.03	0.85	24	16	8	28	22	6
8.98	0.95	25	18	7	20	11	9
11.48	1.06	14	9	5	20	16	4
14.68	1.17	12	8	4	14	11	3
18.76	1.27	4	4	0	11	10	1
23.99	1.38	1	1	0	2	1	1
30.67	1.49	1	0	1	0	0	0
39.20	1.59	0	0	0	1	1	0

Particle Size		Low Particle (S. No. 695474)			Thin (S. No. 590331)		
µm	log (µm)	total	Fe	Si	total	Fe	Si
1.26	0.10	33	1	32	138	10	128
1.61	0.21	47	11	36	209	13	196
2.06	0.31	31	5	26	115	14	101
2.63	0.42	24	7	17	127	26	101
3.36	0.53	25	8	17	86	24	62
4.30	0.63	18	6	12	69	21	48
5.50	0.74	12	8	4	76	34	42
7.03	0.85	6	2	4	48	27	21
8.98	0.95	1	0	1	38	26	12
11.48	1.06	1	0	1	10	7	3
14.68	1.17	0	0	0	3	3	0
18.76	1.27	0	0	0	0	0	0
23.99	1.38	0	0	0	1	1	0
30.67	1.49	0	0	0	0	0	0
39.20	1.59	0	0	0	0	0	0

jw/3382

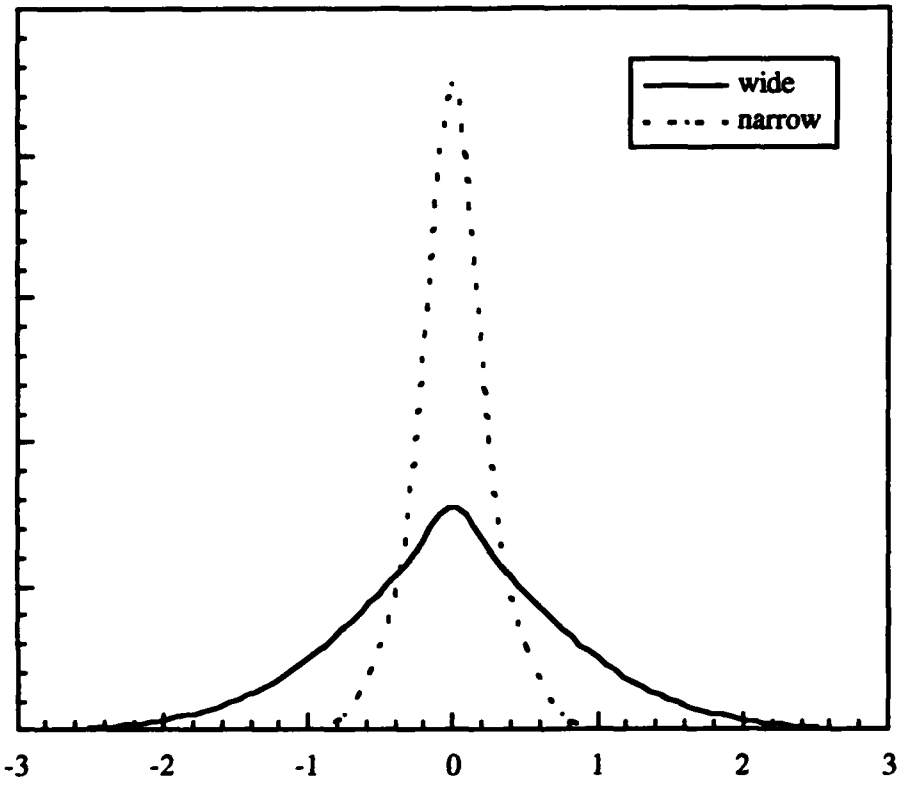

Figure 1.

Comparison of normal distributions with the same mean value, but different standard deviations.

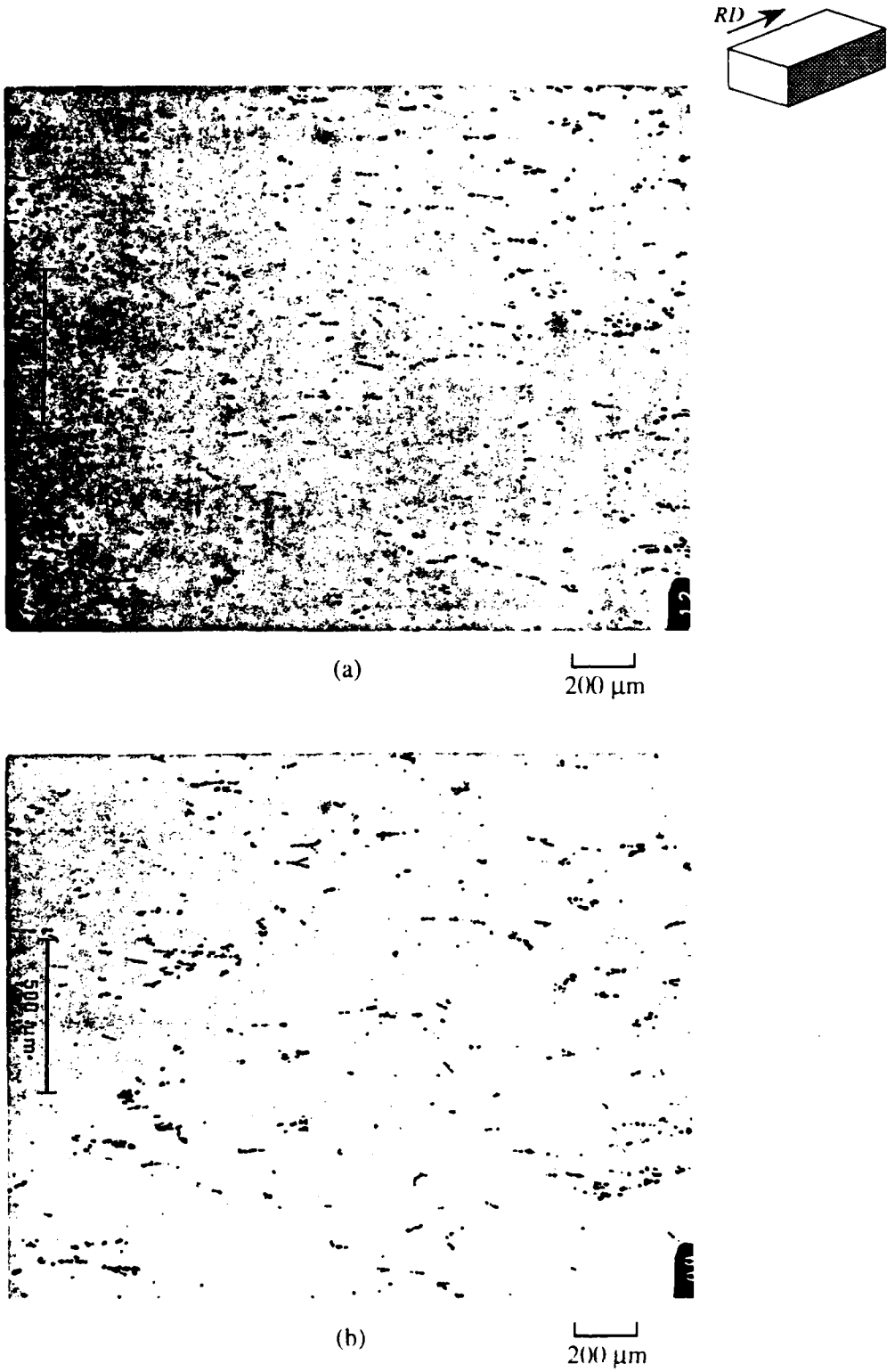

Figure 2. Optical micrographs of constituent particles at T/2 in (a) standard plate S No. 590158 and (b) low porosity plate S. No. 590553.

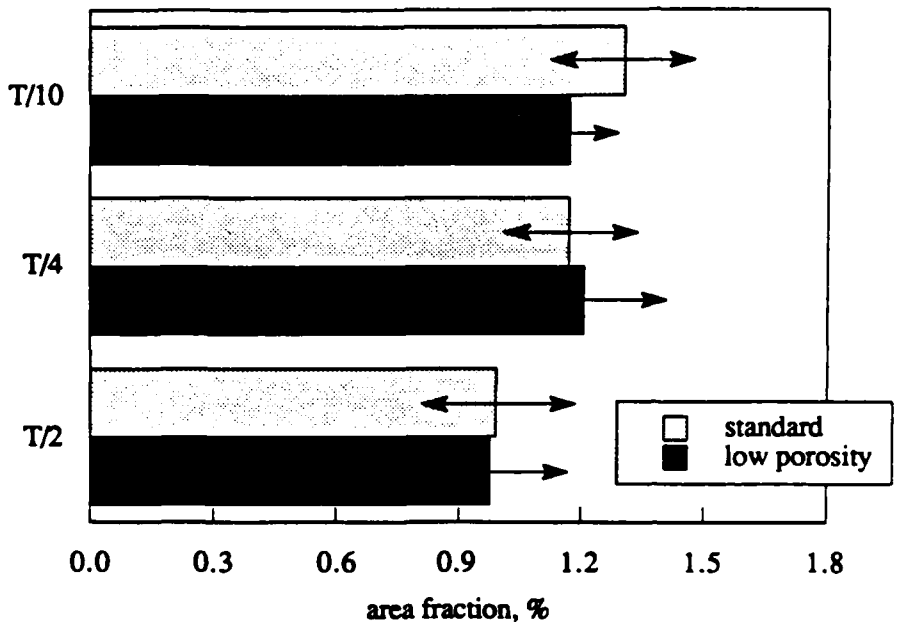

(a)

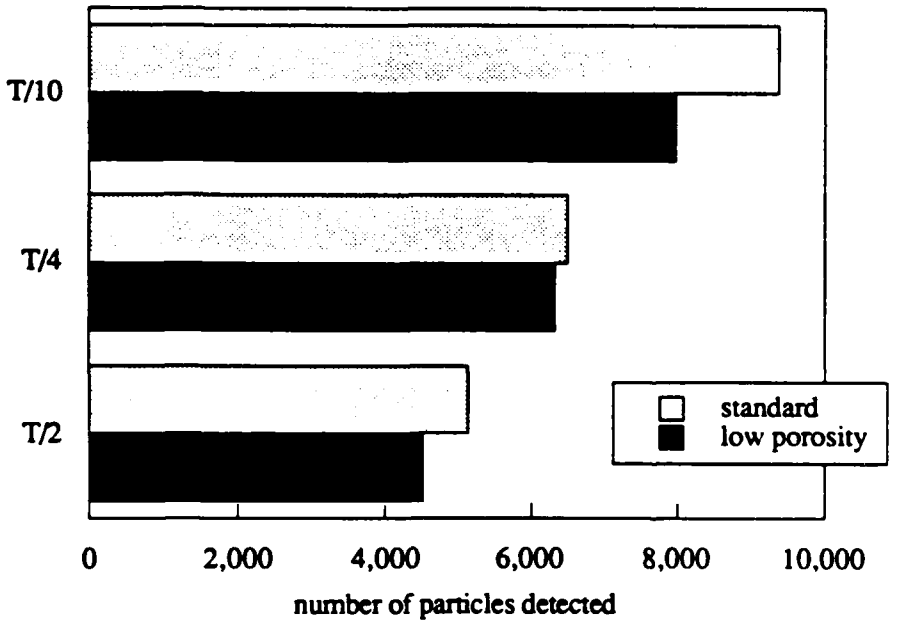

(b)

Figure 3.

Graphs showing the effect of processing parth on (a) particle area fraction, and (b) particle number density at different plate locations.

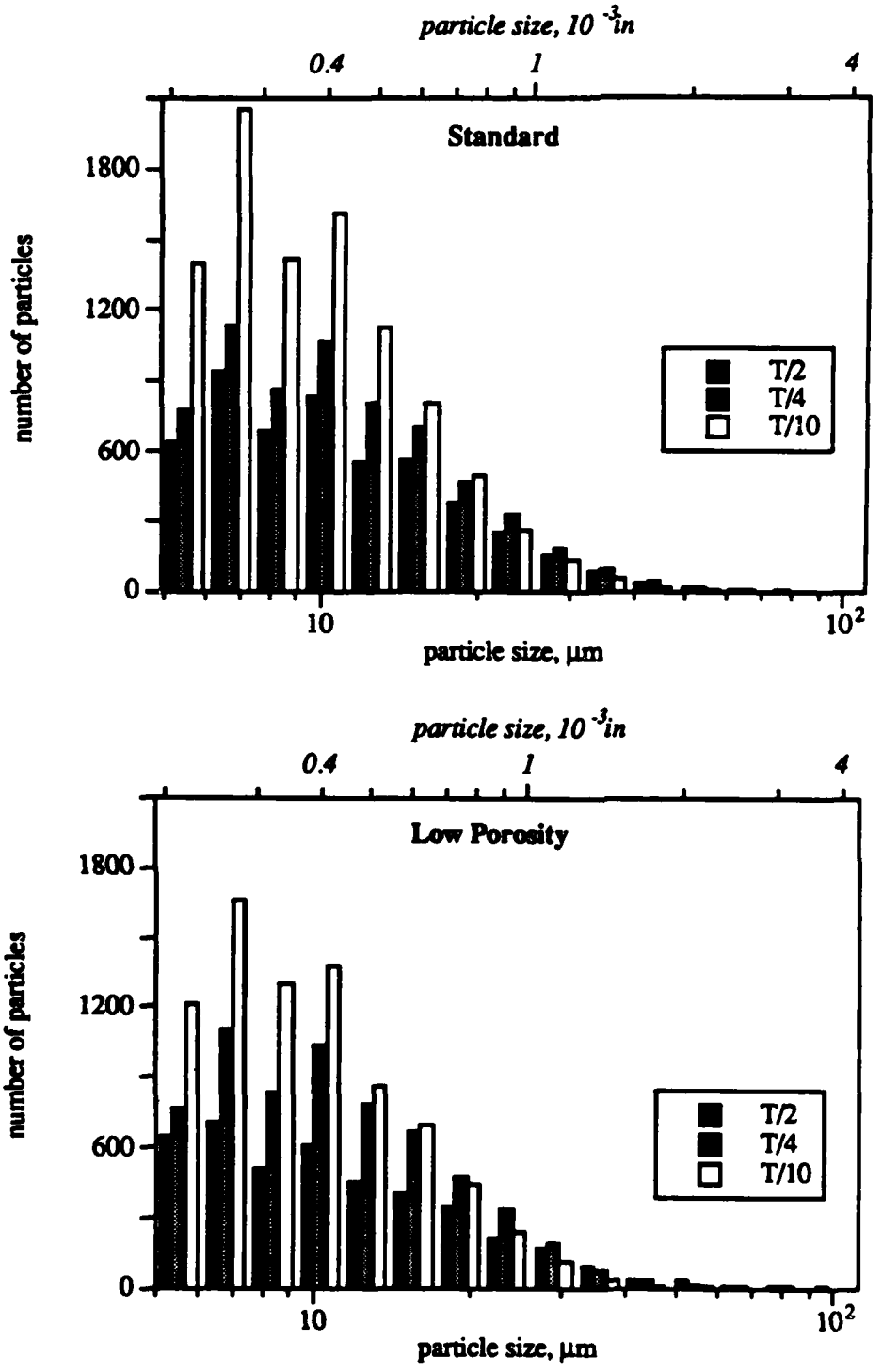

(a)

(b)

Figure 4.

Histograms of particle size on a logarithmic scale for (a) standard and (b) low porosity materials.

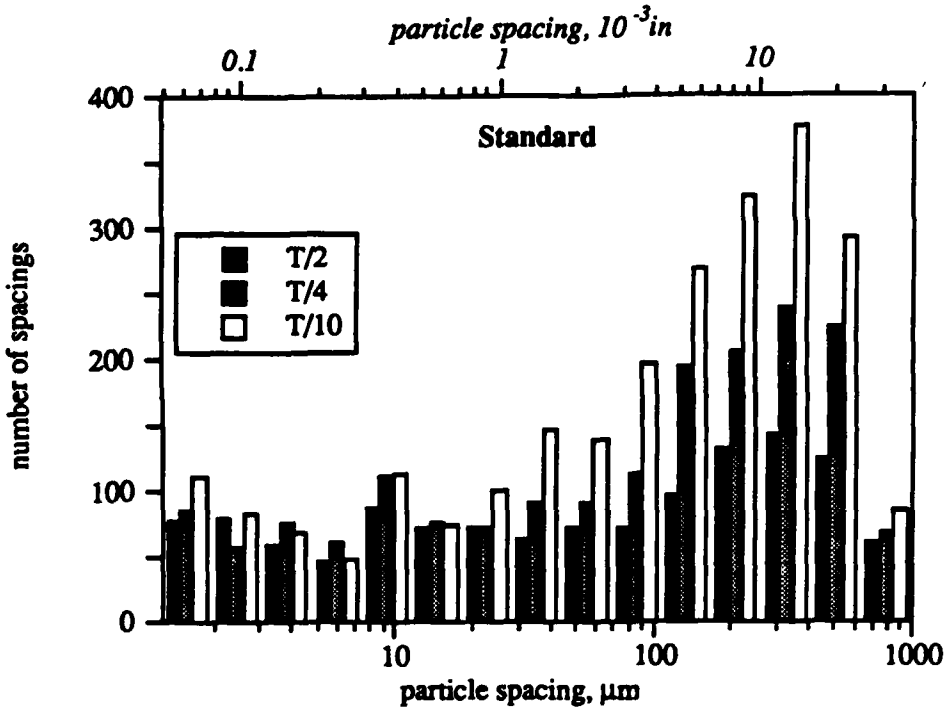

(a)

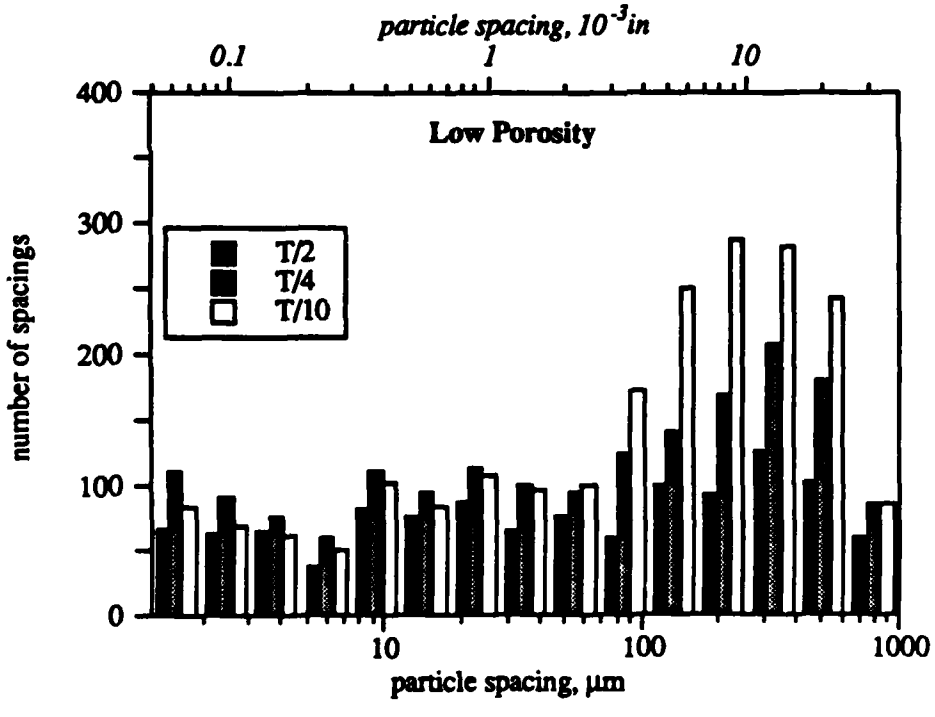

(b)

Figure 5.

Histogram of inter-particle spacing and inter-stringer spacing on a logarithmic scale for (a) standard and (b) low porosity materials.

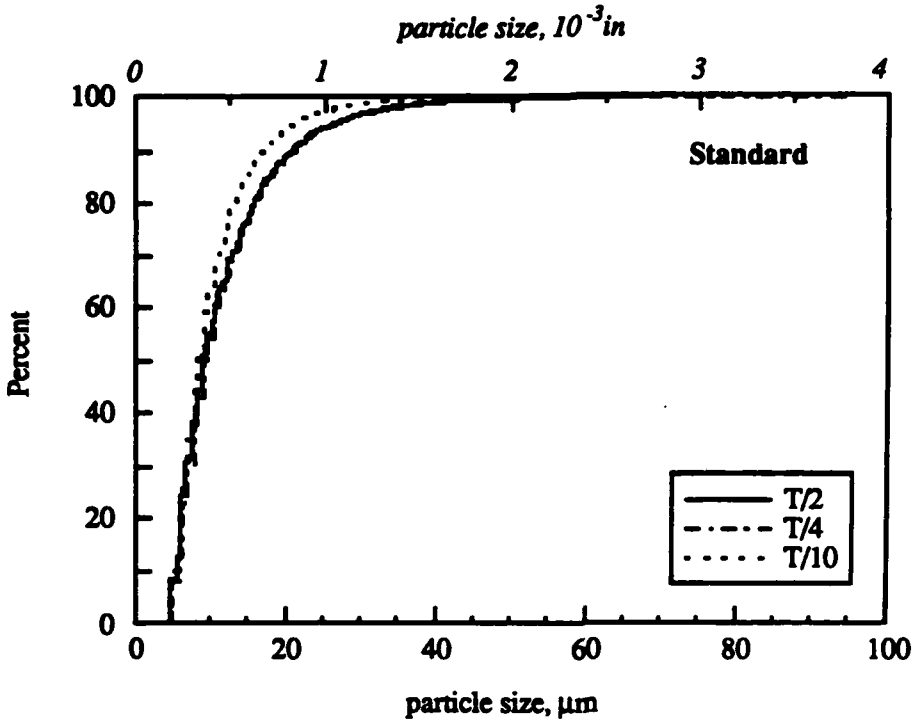

(a)

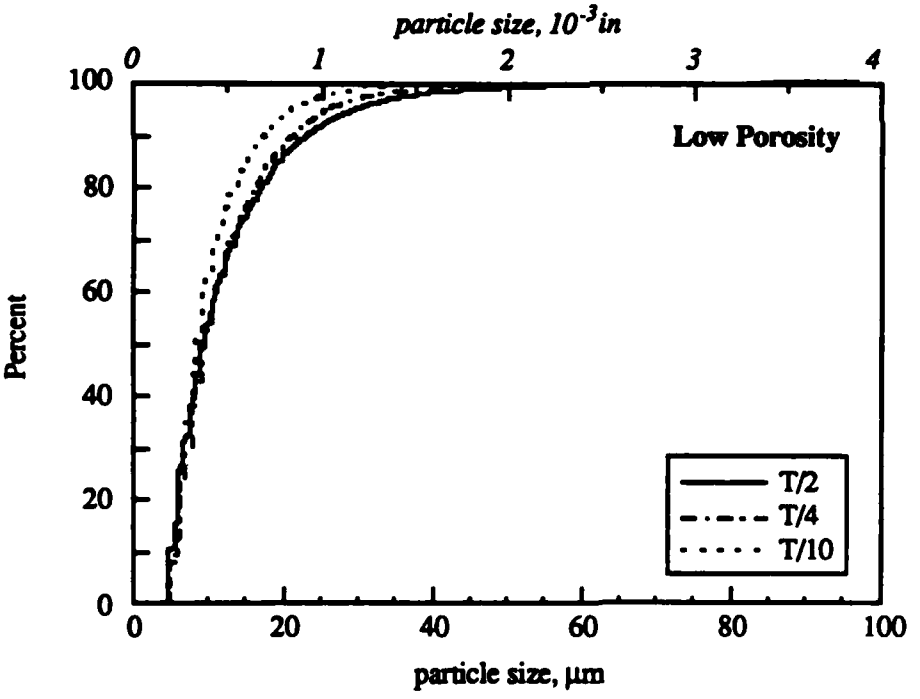

(b)

Figure 6.

Graphs of particle size for (a) standard and (b) low porosity materials.

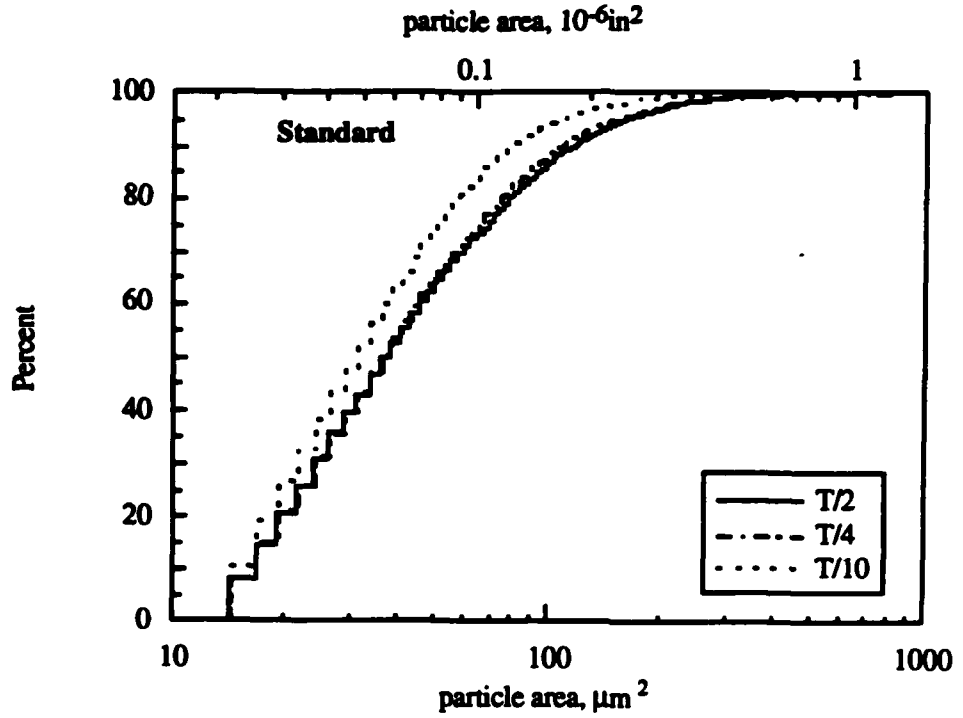

(a)

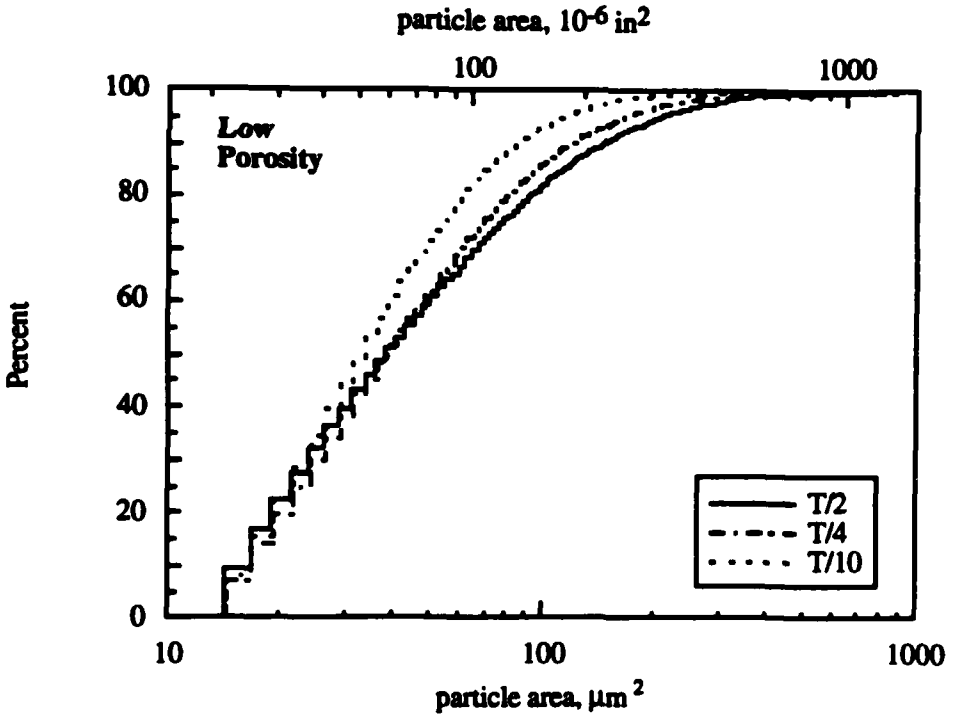

(b)

Figure 7.

Graphs of measured particle area for (a) standard and (b) low porosity materials at different thickness locations.

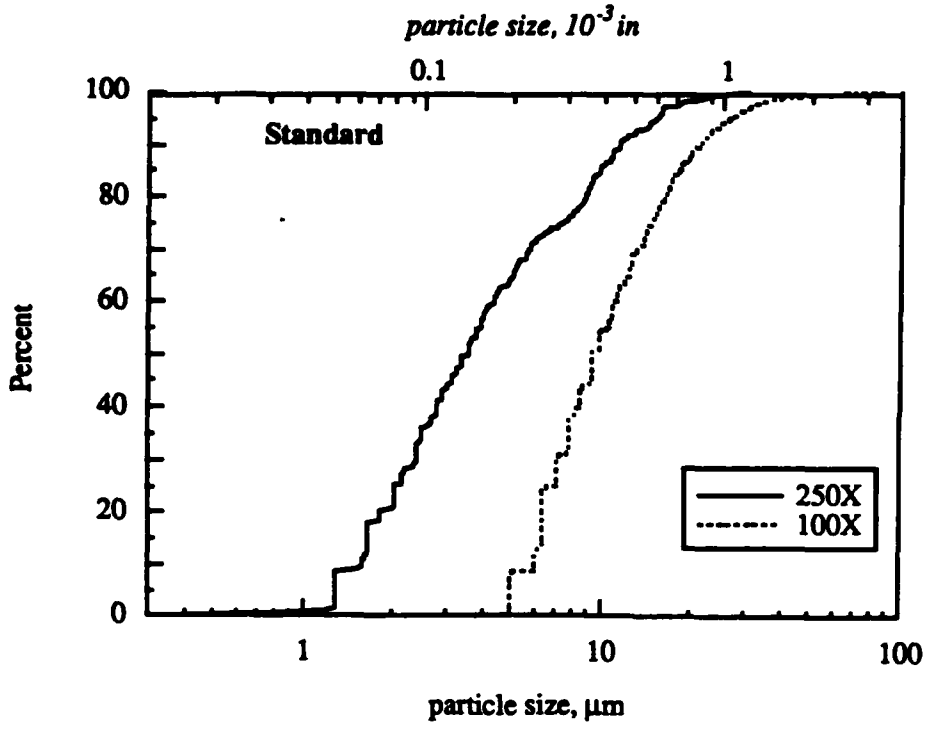

(a)

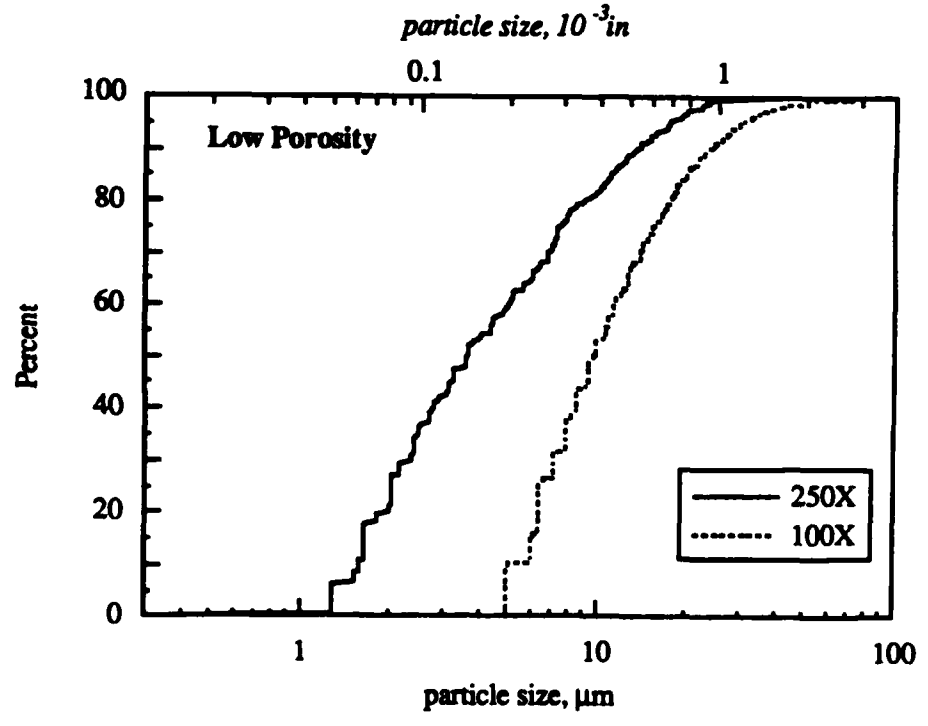

(b)

Figure 8.

Plots of particle size at the T/2 location in (a) standard and (b) low porosity material measured at two different magnifications. Specimen area was 1.2 mm^2 at 250X and 31 mm^2 at 100X.

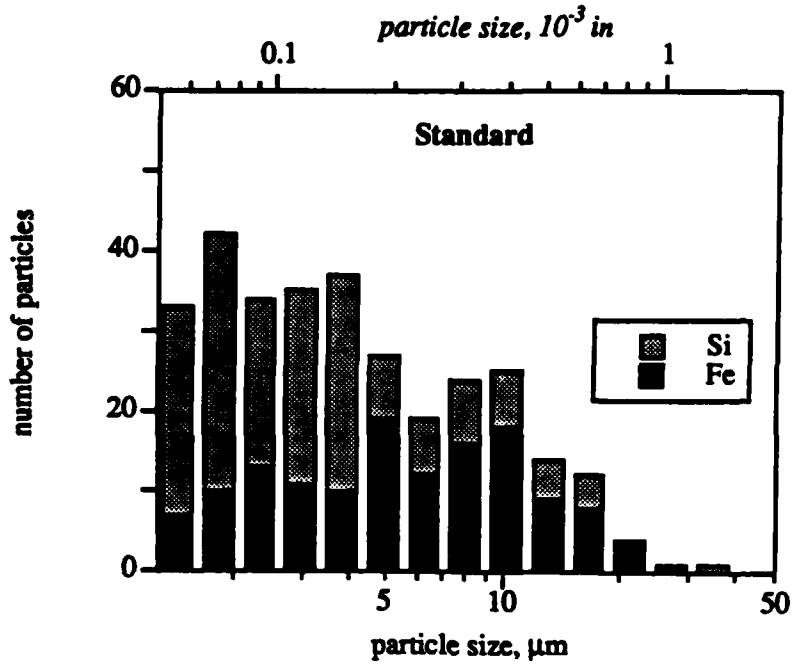

(a)

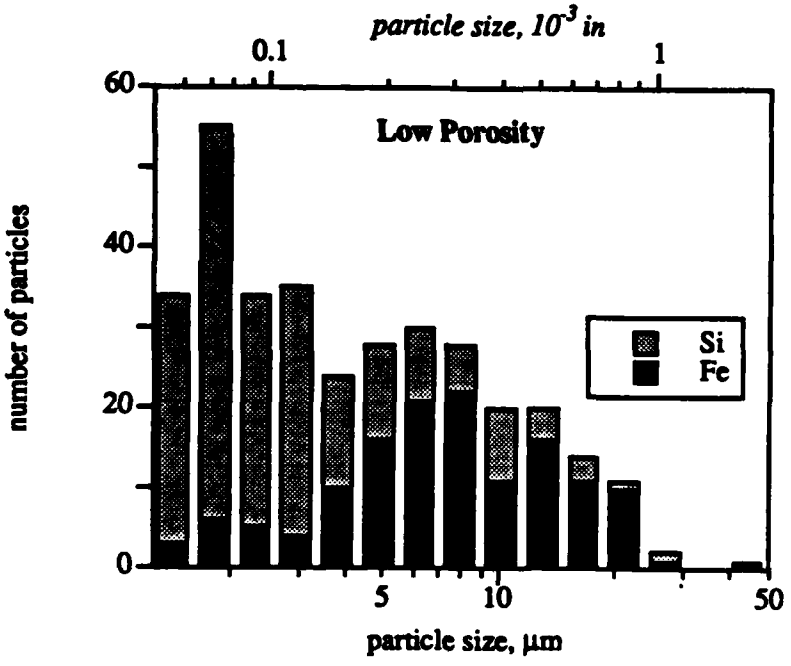

(b)

Figure 9.

Histograms of total, Fe- and Si-containing particle size on a logarithmic scale for (a) standard and (b) low porosity materials.

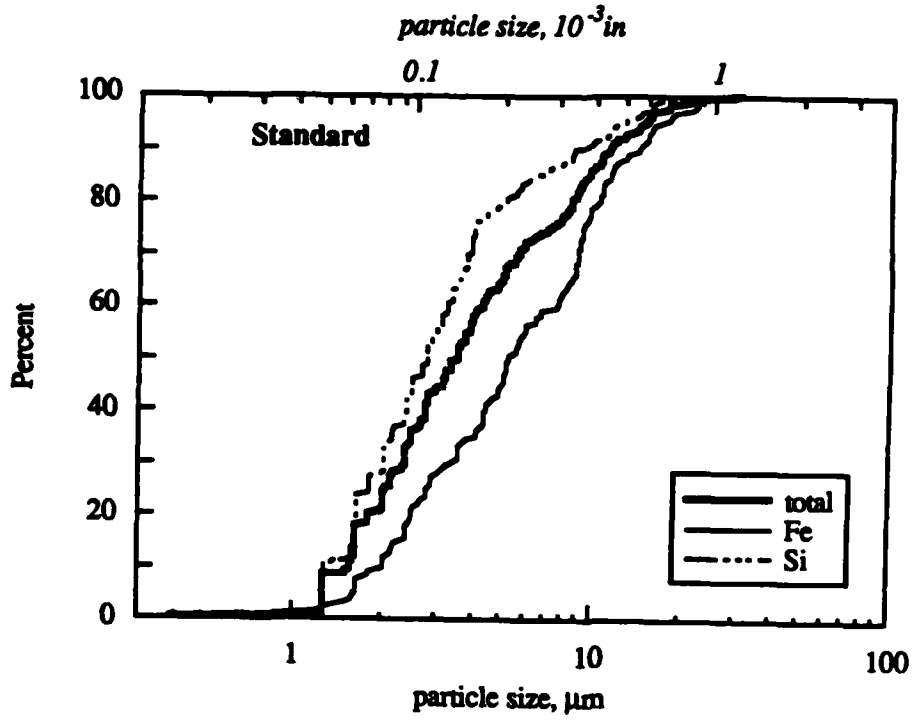

(a)

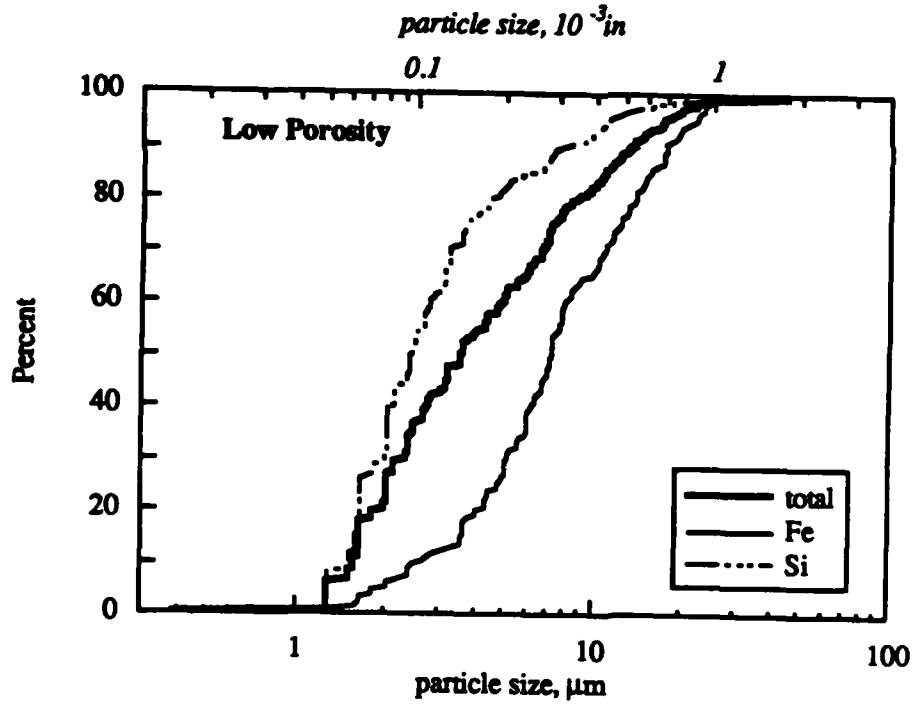

(b)

Figure 10.

Plots of total, Fe- and Si-containing particle sizes for (a) standard and (b) low porosity materials.

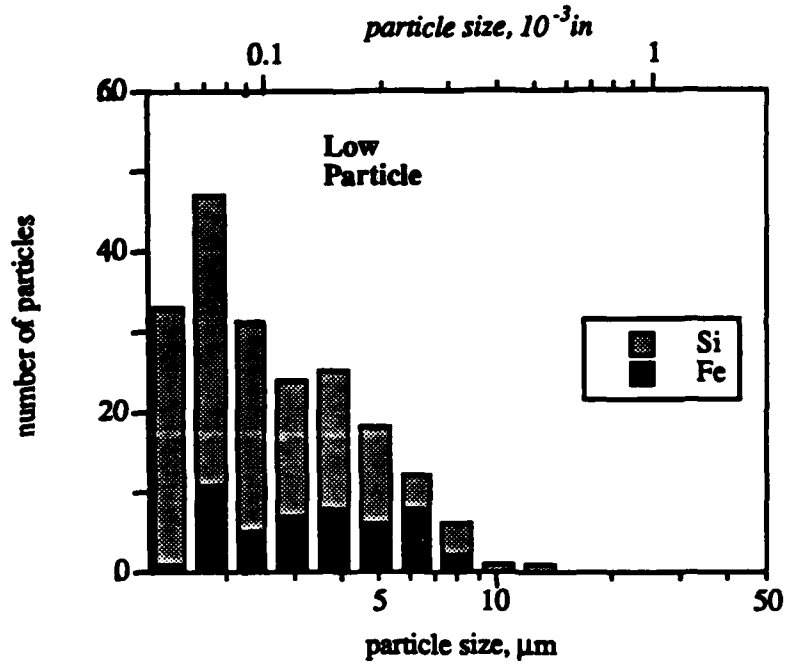

(a)

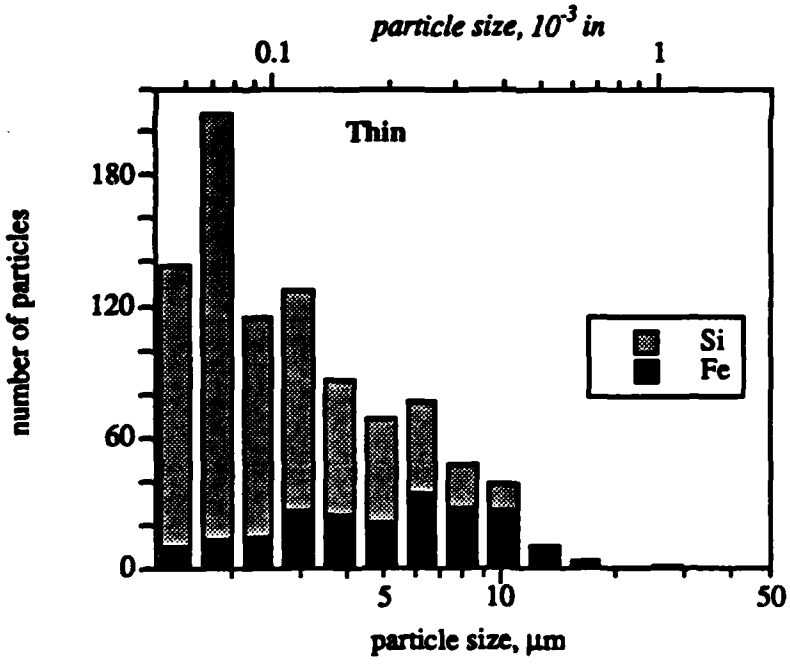

(b)

Figure 11.

Histograms of total, Fe- and Si-containing particle size on a logarithmic scale for (a) low particle and (b) thin plate.

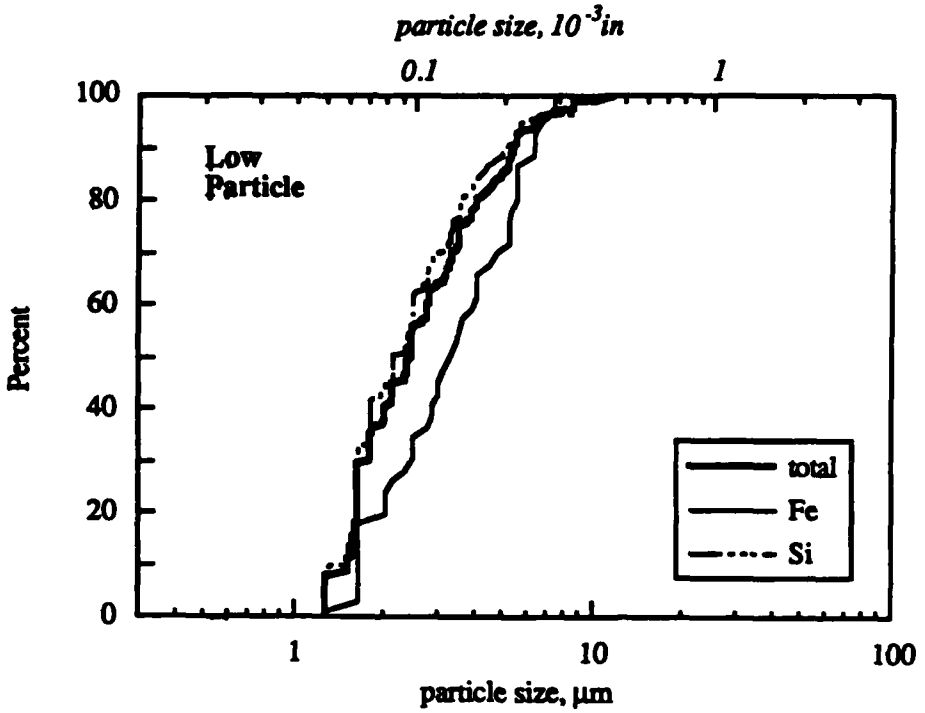

(a)

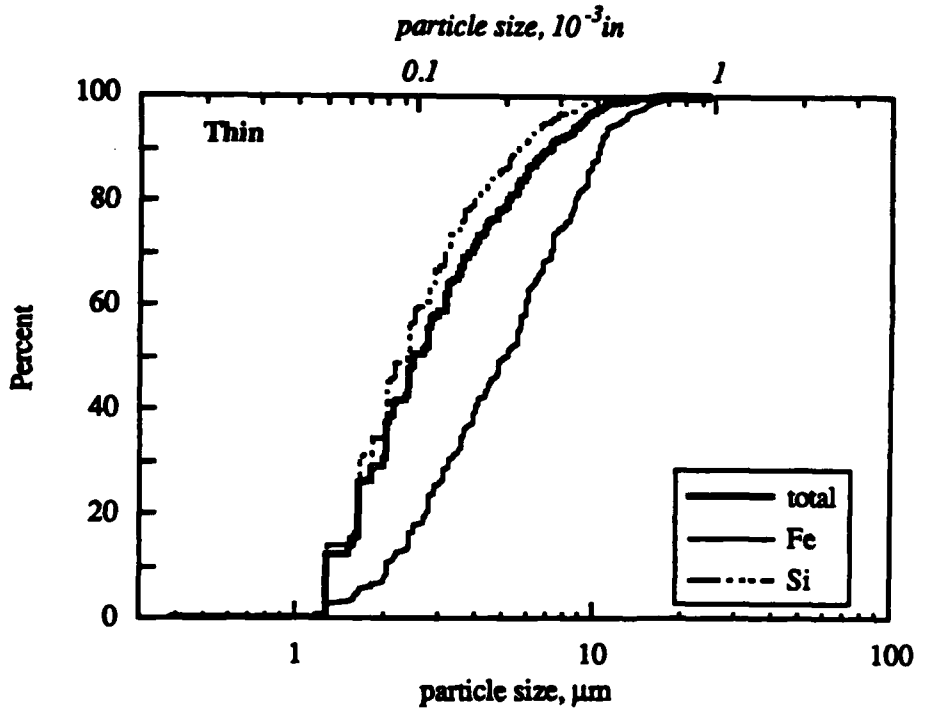

(b)

Figure 12.

Plots of total, Fe- and Si-containing particle sizes for (a) low particle and (b) thin plate.